# Evidence of solid Earth influence on stability of the marine-terminating Puget Lobe of the Cordilleran Ice Sheet

Marion McKenzie[1], Lauren E Miller[2], Allison Lepp[2], and Regina DeWitt[3]

[1]Colorado School of Mines
[2]University of Virginia
[3]East Carolina University

November 3, 2023

### Abstract

Understanding drivers of marine-terminating ice sheet behavior is important for constraining ice contributions to global sea-level rise. In part, the stability of marine-terminating ice is influenced by solid-Earth conditions at the grounded-ice margin. While the Cordilleran Ice Sheet (CIS) contributed significantly to global mean sea level during its final post-Last Glacial Maximum (LGM) collapse, the drivers and patterns of retreat are not well constrained. Coastal outcrops in the deglaciated Puget Lowland of Washington state - largely below sea level during glacial maxima, then uplifted above sea level via glacial isostatic adjustment (GIA) - record late Pleistocene history of the CIS. The preservation of LGM glacial and post-LGM deglacial sediments provides a unique opportunity to assess variability in marine ice-sheet behavior of the southernmost CIS. Based on paired stratigraphic and geochronological work with a newly developed marine-reservoir correction for this region, we identify that the late-stage CIS experienced stepwise retreat into a marine environment about 12,000 years before present, placing glacial ice in the region for about 3,000 years longer than previously thought. Stand-still of marine-terminating ice for a millenia, paired with rapid vertical landscape evolution, was followed by continued retreat of ice in a subaerial environment. These results suggest rapid rates of solid Earth uplift and topographic support (e.g., grounding-zone wedges) stabilized the ice-margin, supporting final subaerial ice retreat. This work leads to a better understanding of shallow marine and coastal ice sheet retreat; relevant to sectors of the contemporary Antarctic and Greenland ice sheets and marine-terminating outlet glaciers.

### Hosted file

977889_0_art_file_11532758_s3753f.docx available at https://authorea.com/users/671812/articles/674999-evidence-of-solid-earth-influence-on-stability-of-the-marine-terminating-puget-lobe-of-the-cordilleran-ice-sheet

# Evidence of solid Earth influence on stability of the marine-terminating Puget Lobe of the Cordilleran Ice Sheet

**Marion A. McKenzie[1*], Lauren E. Miller[1], Allison P. Lepp[1], and Regina DeWitt[2]**

[1]Department of Environmental Sciences, University of Virginia, 291 McCormick Rd., Charlottesville, VA, USA 22904 [2]Department of Physics, East Carolina University, 1000 E. 5th St., Greenville, NC, USA 27858-4353

Corresponding author: Marion McKenzie (marion.mckenzie@mines.edu)

[*]Author now affiliated with the Geology and Geological Engineering Department, Colorado School of Mines, 1105 Illinois St., Golden, CO, USA 80201

**Key Points:**

- Solid Earth uplift is capable of stabilizing marine-terminating ice streams and seen in stratigraphy across the Puget Lowland.
- The Puget Lobe of the Cordilleran Ice Sheet was present in the Puget Lowland until at least 12,100 calendar years before present.
- A newly developed marine reservoir for the Puget Lowland is found to be 264 $^{14}C$ years or 50 calendar years before present.

## Abstract

Understanding drivers of marine-terminating ice sheet behavior is important for constraining ice contributions to global sea-level rise. In part, the stability of marine-terminating ice is influenced by solid-Earth conditions at the grounded-ice margin. While the Cordilleran Ice Sheet (CIS) contributed significantly to global mean sea level during its final post-Last Glacial Maximum (LGM) collapse, the drivers and patterns of retreat are not well constrained. Coastal outcrops in the deglaciated Puget Lowland of Washington state - largely below sea level during glacial maxima, then uplifted above sea level via glacial isostatic adjustment (GIA) - record late Pleistocene history of the CIS. The preservation of LGM glacial and post-LGM deglacial sediments provides a unique opportunity to assess variability in marine ice-sheet behavior of the southernmost CIS. Based on paired stratigraphic and geochronological work with a newly developed marine-reservoir correction for this region, we identify that the late-stage CIS experienced stepwise retreat into a marine environment about 12,000 years before present, placing glacial ice in the region for about 3,000 years longer than previously thought. Stand-still of marine-terminating ice for a millenia, paired with rapid vertical landscape evolution, was followed by continued retreat of ice in a subaerial environment. These results suggest rapid rates of solid Earth uplift and topographic support (e.g., grounding-zone wedges) stabilized the ice-margin, supporting final subaerial ice retreat. This work leads to a better understanding of shallow marine and coastal ice sheet retreat; relevant to sectors of the contemporary Antarctic and Greenland ice sheets and marine-terminating outlet glaciers.



## Plain Language Summary

Glaciers that deposit ice directly into the ocean are capable of losing large amounts of ice that contribute to global sea level rise. The surface that glaciers sit on can influence how quickly ice is lost to the ocean. Vertical movement of solid Earth, as a result of large ice losses, is capable of stopping glacial retreat in an ocean environment. Records of the interaction between Earth and glacial ice movement are contained in the sediments along the coast of the Puget Lowland in Washington state. This work finds that glacial ice in the Puget Lowland, from 20,000 years ago, was present in the area about 3,000 years longer than previously thought. We also interpret that solid Earth movement provided stability to this marine-terminating glacial ice for about 1,000 years. These results are significant because this landscape is similar to parts of the Greenland Ice Sheet and the Antarctic Peninsula, indicating that the interactions seen in this area are applicable to modern glaciated regions.


## 1 Introduction

The terrain and substrate geology beneath ice sheets have the potential to affect the behavior of the overriding ice; they can influence ice flow organization, velocity, and margin positions (Weertman, 1974; Clarke et al., 1977; Clark, 1994; Whillans & van der Veen, 1997; Cuffey & Paterson, 2010; Jamieson et al., 2012; Margold et al., 2015). Coupled ice sheet and solid Earth models indicate that glacial isostatic adjustment (GIA) can stabilize marine-based grounding lines (van der Wal et al., 2015; Whitehouse et al., 2019; Wan et al., 2022) but this relationship has yet to be tested empirically. Due to the difficulty in observing subglacial conditions and solid Earth dynamics beneath modern ice sheets, we turn to the deglacial sediment record of the extinct Cordilleran Ice Sheet (CIS) in the Puget Lowland. Specifically, we consider the marine-based southernmost part of the CIS, the Puget Lobe, which most recently advanced across the Puget Lowland during the Last Glacial Maximum (~20,000 years ago; Mullineaux et al., 1965; Easterbrook et al., 1967; Easterbrook, 1969; Porter & Swanson, 1998). The Puget Lowland records vertical land change due to tectonics and glacial isostatic adjustment (GIA) from Puget Lobe advance and retreat in the region, making it an ideal location to study influence of solid Earth on ice-sheet behavior and post-glacial landscape evolution. Topographic similarities between the Puget Lowland and Greenland indicate the deglacial history of the Puget Lobe may be an appropriate analog for studying contemporary Greenland Ice Sheet outlet glaciers (Eyles et al., 2018). Additionally, the ice histories and solid Earth properties, such as flexural thickness of the lithosphere and mantle viscosity, in this region are similar to that of the Antarctic Peninsula (Nield et al., 2014; Whitehouse et al., 2019). Contributing to understanding the role of topography and solid-Earth conditions on marine-based glacial ice can lead to development of a process-based model on marine-terminating retreat of modern ice sheets. The findings from this work are relevant to modern glacial systems and have implications for timing of CIS contribution to global sea level as well as routes and timing of human migration into the Americas (Mandryk et al., 2001; Goebel et al., 2011; Lesnek et al., 2018).

### 1.1 Regional Context

The Puget Lowland of Washington state has been glaciated at least six times throughout the Quaternary as a result of CIS advance and retreat in the region. Glaciations occurred during marine isotope stage (MIS) 6 (~97,000 to 150,000 years ago; Easterbrook, 1969), MIS 4 (80,000 ± 20,000 years; Easterbrook et al., 1967; Easterbrook. 1969), and towards the end of MIS 2 (~17,500 cal. year BP; Mullineaux et al., 1965; Porter & Swanson, 1998). Existing geochronology places final deglaciation of the Puget Lowland around 16,500 calendar years before present (cal. yr. B.P.) (Easterbrook, 1992; Dethier et al., 1995; Swanson & Caffee, 2001). Yet, the lack of detailed stratigraphic context for age constraints and absence of a local marine reservoir correction (MRC) have left uncertainties in the exact timing of ice retreat. Nonetheless, based on similarities in previously published radiometric ages, it is suggested that marine incursion drove rapid lift-off and northward retreat of the Puget Lobe (Thorson, 1980, 1981; Waitt and Thorson, 1983; Booth, 1987; Booth et al., 2003). However, there are variable records of deglacial stratigraphy across the region (Powell, 1980; Pessl et al., 1981; Domack, 1984; Demet et al., 2019), and the presence of ice-marginal landforms indicate periodic stand-still in ice margin during retreat (Simkins et al., 2017; Demet et al., 2019). Subsequently, the need to clarify spatiotemporal details of ice retreat patterns and drivers of Puget Lobe retreat persists.

The magnitude of landscape emergence due to GIA in the Puget Lowland may have been as high as 10 cm $a^{-1}$ during early deglaciation (Dethier et al., 1995), likely due to the elastic solid-Earth response to unloading (c.f. Whitehouse, 2018). This rate of GIAinduced uplift suggests relative sea-level fall in the Puget Lowland outpaced rapid global sea-level rise, leading to emergence of the landscape from below to above sea level during the end of the LGM (Shugar et al., 2014; Yokoyama & Purcell, 2021). Both pre-existing topography and GIA could have periodically stabilized the Puget Lobe during retreat, as suggested for contemporary ice sheets (Durand et al., 2011; Favier et al., 2016; Alley et al., 2021; Robel et al., 2022), highlighting the importance of elucidating the role of both conditions on ice-sheet behavior.

**1.2 Relevance to solid Earth dynamics and modern ice sheets and glaciers**

Based on modelled evidence of GIA control on ice behavior in analogous Antarctic Peninsula glacial catchments (Nield et al., 2014; Whitehouse et al., 2019), in addition to previously identified geomorphic evidence of ice-margin stand still in the Puget Lowland (Simkins et al., 2017; Demet et al., 2019), we hypothesize that landscape position above and below sea level, due to loading and unloading of the solid Earth, influenced ice-margin positions and led to punctuated retreat of the CIS during the late Pleistocene. In the central Puget Lowland, Whidbey Island spans nearly 100 kilometers in distance along the North-South direction of glacial ice movement and hosts extensive coastal bluff features (Figure 1B). The outcrops, composed of glacial and interglacial sediments, preserve details of ice advance and retreat across the formerly marine landscape, as well as landscape transitions that took place coeval with deglaciation. Except for localized tectonic deformation of surficial sediments (Sherrod et al., 2008), local LGM and subsequent deglacial deposits appear to have little post-depositional reworking (Booth & Hallet, 1993; Kovanen & Slaymaker, 2004; Eyles et al., 2018; Demet et al., 2019; McKenzie et al., 2023).

In this work, decimeter-scale stratigraphic and sedimentological assessments are complemented by accelerator mass spectrometry radiocarbon ($^{14}C$) and optically stimulated luminescence (OSL) dating. While these two dating methods have been utilized in this region for decades (e.g., Rigg and Gould, 1957; Leopold et al., 1982; Easterbrook, 1992; Anundsen et al., 1994; Dethier et al., 1995; Swanson and Caffee, 2001), our hypothesis of the relationship and timing of landscape emergence in relation to ice retreat and periodic stabilization of ice retreat has not been directly assessed. Therefore, the application of advances in geochronology paired with a high-resolution stratigraphic assessment of Whidbey Island is a novel approach to elucidating the ice retreat and land emergence across the region.

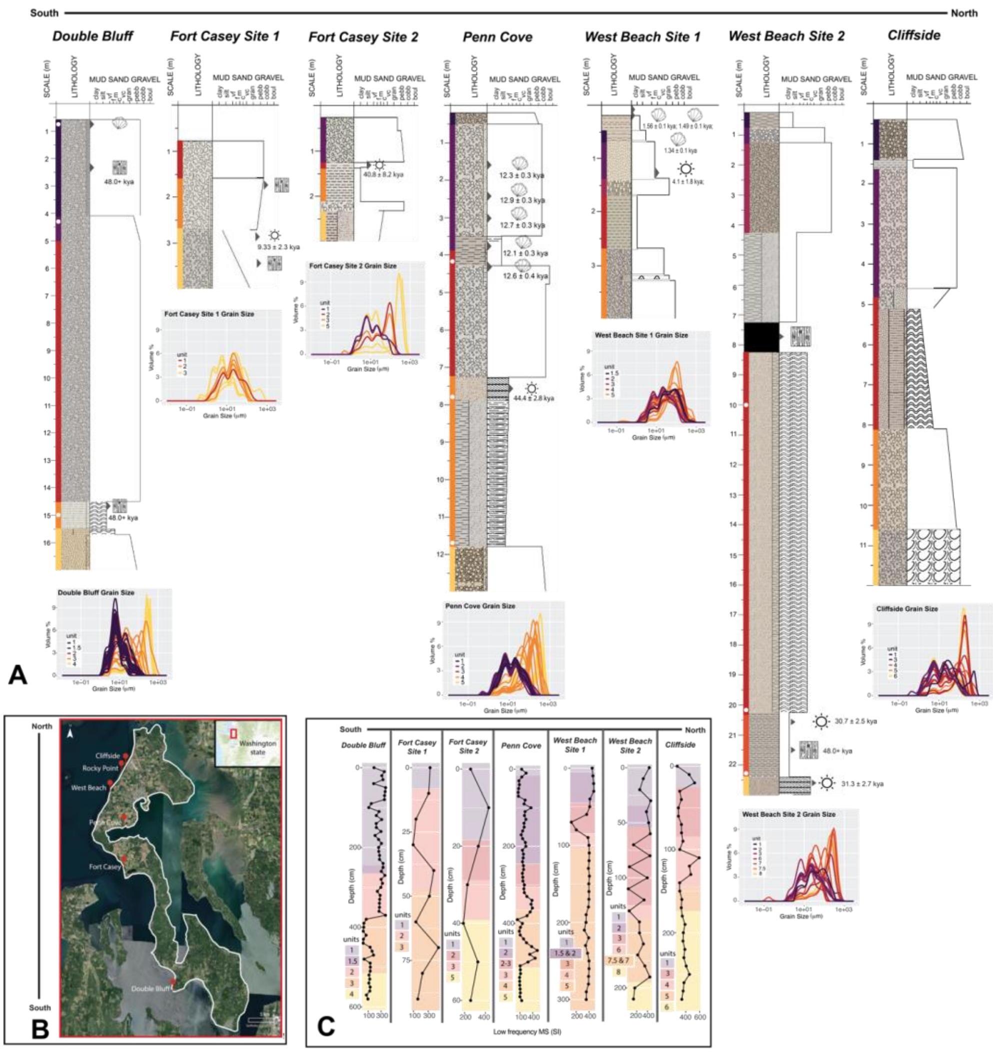


**Figure 1.** A) Outcrop sites from south to north: Double Bluff, Fort Casey 1, Fort Casey 2, Penn Cove, West Beach Site 1, West Beach Site 2, and Cliffside represented by stratigraphic column with collected radiocarbon and OSL and grain size data below. Colors alongside stratigraphic units indicate gran size measurement correlations. White dots indicate changes to site collection of samples. B) Regional inset map with sites labelled south to north . C) Magnetic susceptibility values for each site, listed south to north, and colored boxes indicate stratigraphic unit correlations to values.

### 1.3 Contextualization of Outcrop Research in the Puget Lowland

Over the last six decades, this region has been studied with multiple approaches, varying resolutions, and differing classification methods. Therefore, to provide continuity between our analysis and prior work on final glacial-ice occupation and post-glacial landscape evolution in the Puget Lowland, we provide a summary of stratigraphic units thought to record pre-LGM, LGM, and post-LGM deglaciation and landscape evolution in supplement text (Test S1).

## 2 Materials and Methods

### 2.1 Sedimentology and stratigraphy

Samples were collected from Whidbey Island outcrops a) Double Bluff, b) Fort Casey, c) Penn Cove, d) West Beach, and e) Cliffside at 10-cm intervals (Figure 1B; Table S1) with additional subsamples collected from units with laminations, lenses, or rip-up clasts. Thin (~ <0.5cm thick) horizontally continuous layers are referred to as laminations, while less continuous layers that pinch out are referred to as a lens (e.g., Figure S1). Over 300 discrete bulk sediment samples were analyzed at the University of Virginia for grain size and magnetic susceptibility (MS). An additional 15 peat, wood, and marine shell samples were excavated for radiocarbon dating. Grain size analyses were conducted via a BetterSize S3 Plus Particle analyzer on sample matrix material (material ≤ 3 mm) and MS measurements were collected with a Bartington MS2 magnetic susceptibility meter. MS values provide information about amount and size of magnetic grains in each sample, elucidating continuity and source of biogenic and lithogenic deposits (Thompson and Oldfield, 1986; Verosub and Roberts, 1995; Rosenbaum, 2005; Hatfield et al., 2017; Reilly et al., 2019). Results of the Whidbey Island stratigraphy are presented according to latitudinal location, starting with the southernmost site, Double Bluff, followed by the Fort Casey Sites, Penn Cove, West Beach sites, and ending with the northernmost Cliffside and Rocky Point sites.

### 2.2 Accelerator Mass Spectrometry radiocarbon analysis

Assuming a constant cosmically produced $^{14}C$ to $^{12}C$ ratio, the variation in this ratio can be used to determine the amount of time since the death of formerly living specimens. Samples were run at the National Oceanographic Sciences Accelerator Mass Spectrometry (NOSAMS) Laboratory at Woods Hole Oceanographic Institute. The unprocessed wood material underwent a series of six to eight acid-base-acid leaches to remove contamination and inorganic carbon prior to combustion. The carbonate shell samples underwent carbonate hydrolysis and resulting carbon combustion reacted with Fe catalyst along vacuum-sealed lines to produce graphite (Goehring et al., 2019). Resulting graphite pellets were pressed into targets and analyzed by accelerator mass spectrometry in addition to standard and processing blanks (Roberts et al., 2019). The AMS measurements determined the ratio of $^{14}C$ to $^{12}C$ in each of the pellets, which was then used to calculate the radiocarbon age using the Libby $^{14}C$ half-life of 5,568 years (Stuiver and Polach, 1977; Stuiver, 1980).

Conversion of radiocarbon years to calendar years BP was conducted using the Int20 curve for terrestrial carbon samples and the Marine20 curve for marine shell samples using the Calib 8.2 interface (Heaton et al., 2020). Marine20 is the baseline marine curve used for Calib 8.2 and is the most up-to-date, internationally agreed marine radiocarbon age calibration curve for non-polar global-average marine records (Heaton et al., 2020). A marine reservoir correction was calculated in Calib 8.2 and applied to all carbonate shell samples using contemporary shells with known pre-1955 (i.e., prior to nuclear bomb testing) collected dates from the Burke Museum in Seattle, Washington. The modern (pre-1955) shells from the Burke Institute range in beach-front collection date from 1911 to 1931 (Table 1) and include species *Modiolus rectus, Musculus niger, Cardita ventricas, Macoma carlottensis, Mya arenaria,* and *Macoma nasuta*. The radiocarbon ages calculated from these specimens range from 815 ± 15 to 925 ± 20 $^{14}$C years. Utilizing the marine reservoir correction curve developed by Calib 8.2, an average marine reservoir correction for this region is 264 $^{14}$C years (50 calendar years BP). While there is a narrow range of marine reservoir effects between 211 and 318 $^{14}$C years, a species-specific effect was not observed (Table 1).

**Table 1.** Radiocarbon sample descriptions and data. Gray rows indicate known-age shells dated to develop MRC.

| Name | Type | Age ± error (RCY) | MRC | Δ13C | Age ± error (cal year BP) | actual age (cal year BP) | NOSAMS Receipt # | NOSAMS Accession # |
|---|---|---|---|---|---|---|---|---|
| WB S1 RCD1 s.h. base U6 | Mollusc | 1290 ± 20 | 278 ± 35 | -0.84 | 1494 ± 137 | n/a | 176236 | OS-164669 |
| WB S1 RCD1 s.h. base U6 clam | Mollusc | 1210 ± 25 | 278 ± 35 | -1.4 | 1563 ± 130 | n/a | 176237 | OS-164670 |
| WB S1 U6 RCD2 | Mollusc | 1450 ± 15 | 236 30 | 0.12 | 1336 ± 112 | n/a | 176238 | OS-164671 |
| PC S3 U3 RCD3 | Mollusc | 13200 ± 75 | 278 ± 35 | 0.44 | 12646 ± 371 | n/a | 176239 | OS-164691 |
| PC S3 U4 RCD5 | Mollusc | 13000 ± 75 | 271 ± 35 | -0.31 | 12305 ± 327 | n/a | 176240 | OS-164692 |
| PC S3 U4 RCD1 a.s. | Mollusc | 13250 ± 75 | 264 ± 36 | 0.13 | 12749 ± 366 | n/a | 176241 | OS-164693 |
| PC S4 U6 RCD1 | Mollusc | 1400 ± 20 | 264 ± 36 | | 1390 ± 114 | n/a | 171379 | OS-160221 |
| PC S3-4 RCD2 | Mollusc | 12900 ± 55 | 264 ± 36 | | 12147 ± 293 | n/a | 171380 | OS-160222 |
| PC S3 RCD4 | Mollusc | 13200 ± 55 | 264 ± 36 | | 12674 ± 334 | n/a | 171381 | OS-160223 |
| PC S3 U4 RCD3 | Mollusc | 13300 ± 75 | 216 ± 30 | 0.33 | 12923 ± 343 | n/a | 176242 | OS-164694 |
| WB S2 U1 RCD1 | Plant/Wood | > 48000 | | -23.48 | | n/a | 176243 | OS-164850 |
| PC S4 U6 RCD2 | Mollusc | 1720 ± 15 | 236 ± 30 | -0.06 | 1087 ± 145 | n/a | 176244 | OS-164695 |
| DB S3 RCD1 U4 | Plant/Wood | > 46700 | | | | n/a | 171378 | OS-160371 |
| DB S5 RCD1 U7 | Plant/Wood | > 48000 | | -28.62 | | n/a | 176245 | OS-164851 |
| Mo. r. 6298-1 | Mollusc | 840 ± 15 | 236 ± 30 | 0.15 | 1872 ± 145 | 91 | 176246 | OS-164743 |
| Mu. n. 3320-1 | Mollusc | 860 ± 25 | 253 ± 51 | 1.36 | 1860 ± 148 | 110 | 176247 | OS-164744 |
| Mu. n. 3320-2 | Mollusc | 925 ± 20 | 318 ± 40 | 1.42 | 1866 ± 145 | 110 | 176248 | OS-164745 |
| Ca.v. 13329-1 | Mollusc | 875 ± 20 | 270 ± 40 | 0.49 | 1867 ± 145 | 104 | 176249 | OS-164746 |
| Ca. v. 13329-2 | Mollusc | 890 ± 15 | 285 ± 30 | 1.74 | 1871 ±144 | 104 | 176250 | OS-164747 |
| Ma. c. 3348-1 | Mollusc | 895 ± 15 | 288 ± 30 | 0.85 | 1870 ± 143 | 110 | 176251 | OS-164748 |
| Ma. c. 3348-2 | Mollusc | 890 ± 20 | 283 ± 40 | 0.05 | 1866 ± 145 | 110 | 176252 | OS-164749 |
| My. a. 3427-1 | Mollusc | 905 ± 15 | 298 ± 30 | 0.83 | 1870 ± 143 | 110 | 176253 | OS-164750 |
| My. a. 3427-2 | Mollusc | 850 ± 20 | 243 ±40 | 0.74 | 1866 ± 145 | 110 | 176254 | OS-164751 |
| Ma. n. 3470-1 | Mollusc | 825 ± 15 | 221 ± 30 | 0.99 | 1872 ± 175 | 91 | 176255 | OS-164760 |
| Ma. n. 3470-2 | Mollusc | 815 ± 15 | 211 ± 30 | 0.39 | 1872 ± 175 | 91 | 176256 | OS-164761 |

### 2.3 Optically stimulated luminescence

In depositional environments, minerals are exposed to radiation from in situ uranium (Ur), thorium (Th), and potassium (K) and cosmic rays (Rhodes, 2011; Duller, 2015). Incoming radiation excites electrons which are trapped in structure deformities of quartz and feldspar grains (Rhodes, 2011). When exposed to sunlight, electrons are released from the traps. In returning to their original states, they emit luminescence and the mineral is reset. Upon burial, trapped electrons re-accumulate, and the amount is proportional to the burial time and the radiation exposure, termed “dose”. The rate of irridation, the “dose rate,” can be calculated from the cosmic flux as well as the U, Th, and $^{40}$K concentrations of the surrounding materials. The OSL signal is proportional to the dose and can be measured by exposing the mineral to light in a controlled setting. An age since burial can be determined by dividing the dose by the dose rate.

Materials from glacial environments present challenges due to the potential of the OSL signal not being fully reset between transport and deposition (Wallinga and Cunningham, 2015). Additionally, extensive overburden pressure from glacial ice has the potential to partially or completely reset OSL signatures, which could provide large error to the final OSL stage (King et al., 2014). Subglacial environments, especially those under ice streams, have a presence of significant meltwater which can saturate sediment pore space and influence quartz and feldspar exposure to radiation at the time of and for an extended period of time after deposition (Wallinga and Cunningham, 2015; Duller, 2013).

While a detailed description of the OSL procedure can be found in supplement text (Text S2), a summary is provided here. In order to avoid pre-mature bleaching of samples, they were collected before sunrise or after sunset, only exposed to low energy red light, and wrapped in dark black plastic before being transported to East Carolina University (ECU) for preparation and processing. Samples were prepared for OSL analysis under dark-room conditions using standard procedures to extract 63-212 μm quartz. Due to feldspar contamination, a post-IR blue SAR procedure was used to measure the quartz equivalent dose (Murray and Wintle, 2000; Wallinga et al., 2002; Wintle and Murray, 2006).

Bulk sediment was collected from outcrops for high-resolution gamma spectrometry measurements and stored for at least 4 weeks prior to measurement. OSL samples were taken at unit boundaries, while dose rate samples were only taken from the same unit as the OSL samples. Therefore, the gamma dose rates reflect the sample unit only and contain no information about adjacent, underlying, or overlying units. Uranium concentrations determined from $^{234}$Th were all significantly higher than concentrations determined from $^{214}$Pb and $^{214}$Bi. We assumed that $^{234}$U was leached out of the sample due to in situ water presence.

The sample ages, calculated in calendar years, were calculated by dividing the dose by the dose-rate (Table S2). For samples with feldspar contamination that showed fading, the ages were corrected as suggested by Auclair et al., (2003). While $^{14}$C ages are reported in kilo years ago (kya) calendar year BP (1955), all OSL ages are reported in kya based on the date of collection (2020). OSL ages in kya can be directly compared to kya cal. BP by subtracting 72 years from the OSL age.

**Table 2.** Dose measurements, dose rate, and OSL age data. Final sample ages are bolded. To directly compare OSL and $^{14}$C ages, it would be necessary to subtract 72 years from the OSL ages. This correction is consierdably smaller than the uncertainty of the ages and can therefore be neglected.

| Sample | grain sizes measured | Dose (Gy) | Dose err (Gy) | fading rate (g) (%/decade) | g err | Gamma dose rate (Gy/ka) | Gamma dose rate error | Beta dose rate (Gy/ka) | Beta dose rate error (Gy/ka) | Internal Beta dose rate (Gy/ka) | internal Beta dose rate error (Gy/ka) | total dose rate (Gy/ka) | total dose rate error (Gy/ka) | Age unfaded (ka) | err | Age after fading (ka) | err |
|---|---|---|---|---|---|---|---|---|---|---|---|---|---|---|---|---|---|
| | | | | | | | | | | | | | | | | | |
| FCS1-OSL1 | 90-125 | 12.13 | 2.82 | 7.1 | 6.1 | 0.33 | 0.03 | 0.61 | 0.03 | 0.18 | 0.07 | 1.30 | 0.09 | **9.3** | 2.3 | minimum age | |
| FCS1-OSL2 | | | | | | | | | | | | | | | | | |
| FCS2-OSL1 | 63-90 | 92.96 | 7.27 | 3.6 | 3.8 | 0.67 | 0.07 | 1.27 | 0.06 | 0.14 | 0.06 | 2.26 | 0.11 | 41.2 | 3.8 | **57** | 16 |
| FCS2-OSL2 | 63-90 | 69.16 | 4.6 | 2.7 | 2.5 | 0.60 | 0.06 | 1.21 | 0.06 | 0.14 | 0.06 | 2.13 | 0.10 | 32.5 | 2.7 | **40.8** | 8.2 |
| | | | | | | | | | | | | | | | | | |
| WBS1-OSL1 | 150-250 | 7.5 | 0.68 | 2.6 | 5.5 | 0.55 | 0.06 | 1.10 | 0.06 | 0.36 | 0.21 | 2.20 | 0.22 | 3.40 | 0.46 | **4.1** | 1.8 |
| WBS1-OSL2 | 90-150 | 11.86 | 0.68 | 0 | | 0.56 | 0.07 | 1.14 | 0.06 | 0.00 | 0.11 | 1.90 | 0.14 | **6.24** | 0.59 | | |
| WBS2-OSL1 | 90-212 | 64.58 | 4.66 | 3.74 | 2.5 | 0.67 | 0.05 | 1.39 | 0.06 | 0.25 | 0.23 | 2.37 | 0.24 | 27.2 | 3.4 | **38.1** | 9.7 |
| WBS2-OSL2 | 90-150 | 70.97 | 4.1 | 0 | | 0.67 | 0.05 | 1.33 | 0.07 | 0.22 | 0.11 | 2.27 | 0.14 | **31.3** | 2.7 | | |
| WBS3-OSL1 | 150-212 | 68.43 | 4.96 | 0 | | 0.62 | 0.05 | 1.20 | 0.05 | 0.34 | 0.04 | 2.23 | 0.08 | **30.7** | 2.5 | | |
| WBS3-OSL2 | 150-212 | 55.9 | 4.77 | 2.99 | 1.7 | 0.73 | 0.06 | 1.42 | 0.06 | 0.25 | 0.07 | 2.47 | 0.11 | 22.6 | 2.2 | **29.2** | 4.6 |
| | | | | | | | | | | | | | | | | | |
| PCS2-OSL1 | 125-150 | 75.47 | 5.77 | 4.54 | 0.28 | 0.49 | 0.04 | 0.97 | 0.04 | 0.45 | 0.07 | 2.05 | 0.10 | 36.8 | 3.3 | **56.6** | 4.1 |
| PCS2-OSL2 | 125-150 | 93.2 | 4.11 | 0 | | 0.50 | 0.04 | 1.02 | 0.05 | 0.45 | 0.07 | 2.10 | 0.10 | **44.4** | 2.8 | | |

## 3 Results

We will be moving through results from the southern-most to the northern-most site. Numerical schemes to describe units at each site are independent and do not correlate between sites. Stratigraphic columns were developed to represent our interpretation of physical data present at several locations across these sites and may not reflect all possible interpretations that have been conducted across Whidbey Island.

### 3.1 Double Bluff

The stratigraphically lower-most unit visible at Double Bluff, Unit 4, is a visually well-sorted sand with sparse rounded gravel lenses. Unit 4 is normally graded with clasts ranging from granule to pebbles with a consistent horizonal long-axis orientation and occasional silt rip-ups from non-visible underlying units. A gradational boundary leads into the overlying sandy silt and fine clayey silt of Unit 3. This unit contains wavy laminations and woody debris dated to be 46.7+ thousand years (kya) cal. BP (i.e., "radiocarbon dead"; Table 1 NOSAMS Receipt #171378). Unit 3 generally fines upwards but with variable matrix grain size modes from 10-500 μm (Figure 1A). Unit 2 is composed of massive diamicton with a clay and fine-silt matrix, marked by a matrix grain size mode of 8 μm and a mix of angular and rounded granule to cobble-sized clasts without a preferred long-axis orientation. There is a gradational contact between Unit 2 and Unit 1. Unit 1 consists of diamicton with a matrix varying between sandy silt and silty sand with woody debris dated to 48.0+ kya cal. BP in age (i.e., "radiocarbon dead"; Table 1 NOSAMS Receipt #176245) and clasts that are predominantly aligned parallel to bedding and evidence of soft-sediment deformation. This uppermost unit has interbedded silt and clay, as well as marine shells in the upper 50 cm of silt that were inaccessible for sampling. MS values in Unit 3 are distinctly lower than the other units (Figure 1A).

### 3.2 Fort Casey

The lower-most visible unit, Unit 3, at Fort Casey Site 1 consists of massive diamicton with a fine-silt and clay matrix and randomly oriented pebble to cobble-sized angular and rounded clasts. Interbedded with the massive diamicton are discrete gravel and sand laminations at the base of Unit 3 and silt and clay laminations with rip ups and woody debris toward the top of Unit 3. Unit 2 consists of fine sand to pebble-size clasts in a sandy silt matrix with vertically oriented and reverse-graded angular clasts. Unit 2 has a remarkably consistent matrix grain size throughout the unit and a minimum OSL age of 9.33 ± 2.3 kya (Table 2 Sample #1) from the upper unit boundary (Figure 1A). This unit also contains sand and silt lenses with mud and plant rip ups (Figure 1A). A gradational boundary leads to Unit 1, which is massive diamicton similar to Unit 3 but with a matrix distinctly lighter in color.

At Fort Casey Site 2, the lower visible unit, Unit 5, contains interbedded clay and sand with reverse grading (Figure 1A). Unit 4, in which no samples were collected, consists of diamicton with concentrated granule to pebble lenses and clay and silt lenses, as well as evidence of soft-sediment deformation. Unit 3 is a massive clay, followed by the Unit 2 layer of silt about 20 cm thick, continuous across an irregular, undulating, and most likely erosional contact. OSL dates at the top of Unit 2 and base of Unit 1 were found to be 40.8 ± 8.2 and 56.6 ± 15.5 kya (Table 2 Samples #3, 2). The overlying Unit 1 is a diamicton with very fine sand to cobble sized angular and rounded clasts. Normal grading is present in the matrix of Unit 1 with fractured (i.e., seemingly crushed) granite clasts.

### 3.3 Penn Cove

The lowest visible unit at this site, Unit 5, comprises a reverse-graded diamicton with a coarsening upward sand matrix and rounded granules and pebbles (Figure 1A). Following a sharp boundary with Unit 5, Unit 4 consists of silt and sand laminations with cross-bedded sands near the top. Unit 4 deposits were OSL dated to ages 56.6 ± 4.1 and 44.4 ± 2.8 kya (Table 2 Samples #10, 11). The grain size modes for Unit 4 matrix are predominantly between 500-700 μm (Figure 1A). An erosional boundary at the top of Unit 4 leads to the massive clayey silt diamicton of Unit 3 with rounded fine- to cobble-size clasts and occasional sandy silt and silt lenses. A gradational boundary separates Units 3 and 2, which is a massive clay diamicton with rounded fine sand to cobble grains and articulated shells. Six shells from Unit 2 were radiocarbon dated with ages spanning 12.9 ± 0.3 to 12.1 ± 0.3 kya cal. BP (Table 1 NOSAMS Receipt #176239-176242, 171380, 171381). Unit 2 also contains sand lenses and wood fragments. Unit 2 has a sharp contact with Unit 1, which consists of normally graded gravel with rounded and angular small to large pebbles with no predominant long-axis orientation. A mode of clay-sized grains is visible in Units 2 and 3 but is not visible in Unit 1 (Figure 1A).

### 3.4 West Beach

At West Beach Site 1, the lowest unit, Unit 5, consists of matrix-supported diamicton with randomly orientated clasts and two matrix grain size modes at 8 and 20 μm (Figure 1A). This unit has a sandy-silt lamination that interrupts the diamicton. The diamicton above the silty-sand lamination, however, contains highly irregular dips and soft-sediment deformation. Unit 5 has a gradational boundary with Unit 4 – a light clay layer deposited on a laterally irregular surface, marked by normal-grading, or fining upward (Figure 1A). Unit 3 consists of a thick, 0.25-m clast-supported gravel layer with poorly sorted fine sand to cobble size clasts. A sharp, horizontally regular contact occurs between Unit 3 to the 0.75 m-thick, well-sorted sand of Unit 2 with OSL ages of 6.2 ± 0.6 and 4.1 ± 1.8 kya (Table 2 Samples #5, 4). Unit 2 has a gradational contact with Unit 1, which is a modern soil on top of a basal shell hash dating between 1.56 ± 0.1 and 1.34 ± 0.1 kya cal. BP (Table 1 NOSAMS Receipt #173237, 176236). MS values are similar throughout Units 5, 4, 2, and 1, but decrease in Unit 3 (Figure 1A).

At the base of West Beach Site 2 are cross-bedded and coarse sand laminations. OSL dates from the lowermost sand in Unit 8 are dated to 31.3 ± 2.7 and 38.1 ± 9.7 kya (Table 2 Sample #7, 6). A gradational contact leads into Unit 7, consisting of silt and clay with radiocarbon-dead woody debris. Unit 6 consists of sand with wavy bedding and silt laminations. No samples were collected from Units 5 and 4, consisting of a peat layer and a unit of sand and silt laminations, respectively. The Unit 3 diamicton matrix coarsens upwards and this unit has many grain size modes between 5 and 70 μm (Figure 1A). Unit 2 consists of diamicton with a fine sand matrix and clasts as large as pebbles and is not spatially continuous throughout the site. A gradational boundary leads into the 0.5 m-thick layer of Unit 1, consisting of predominantly of silt.

### 3.5 Rocky Point, Cliffside

The lowest visible unit at Cliffside, Unit 6, consists of fine sand to cobble-sized rounded clasts. This massive diamicton has no preferential orientation for clast long axes. The matrix changes from clay to sand and includes sediment deformation beneath clasts (Figure 1A). Unit 6 gradationally transitions to Unit 5, which is a normally graded, fine sand to cobble-size clast diamicton. Unit 5 is normally graded gravel lenses containing clasts with consistent horizontal long-axis orientation. Unit 5 gradually transitions into the granule and sand layer of Unit 4, which includes sand and silt lenses within gravel-rich and wavy laminations. Unit 3 intrudes into Unit 4 and consists of a massive diamicton with rounded, cobble-sized clasts. The matrix of Unit 3 has two grain size modes at 5 and 20 μm (Figure 1A). Two of the lower-unit samples for Cliffside Unit 3 were taken from the more southern Rocky Point site as the identified Unit 3 is continuous throughout both sites. Unit 3 gradually transitions into Unit 2, which is a laterally discontinuous light clay unit with silt layers. Unit 1 is comprised of mostly rounded, normally graded crushed material with fine to large cobble size clasts.

## 4 Discussion and Interpretation

We use the sedimentological units described in Section 3 to establish a facies model that encompasses glaciomarine and coastal sedimentary processes and depositional environments (i.e., emergent or submergent landscape). Aided by geochronological constraints, this facies model is applied to the stratigraphic sequences observed at each site to construct a regional history of ice behavior and landscape evolution before, during, and following the LGM (Figure 2).

### 4.1 Facies interpretation

Structureless diamicton with randomly oriented clasts of variable size, roundness, lithology, and a range in matrix size are classified as **glacial till,** or sediments deposited directly by glaciers in the subglacial environment (Boulton and Deynoux, 1981; Sengupta, 2017). Some biological material may be incorporated into glacial till in the form of broken shells or woody fragments. This reworked biogenic material may be incorporated into the ice as it moves across the landscape, therefore radiocarbon ages of biogenic material will be older than glacial occupation. These characteristics are consistent with glaciomarine tills described offshore of West Antarctica (e.g., Kirschner et al., 2012; Prothro et al., 2018; Smith et al., 2019) and western Greenland (Sheldon et al., 2016; O'Regan et al., 2021), as well as glacial tills deposited by the relict British-Irish Ice Sheet (Evans and Thompson, 2010). Lower boundaries of glacial till units are often characterized by erosional contacts, reflecting glacial advance and erosion of pre-existing substrate, and may contain rip-up clasts from underlying units. Due to similarities in structure to formerly identified glacial tills, units classified as (local) LGM glacial till (i.e., Vashon Till) in the Puget Lowland include Unit 2 from Double Bluff, Unit 3 at Fort Casey Site 1, Unit 1 from Fort Casey Site 2, Unit 3 from Penn Cove, Unit 5 from West Beach Site 1, and Unit 6 from Cliffside (Figures 1, 2). Little post-depositional erosion or reworking of this glacial material is consistent with previous work identifying glacial tills in the region (Booth & Hallet, 1993; Kovanen & Slaymaker, 2004; Eyles et al., 2018; Demet et al., 2019).

**Glacial outwash** is characterized as diamicton with a range of well-rounded and some angular clasts with parallel-to-bedding clast orientation that suggests sediment transport via proglacial meltwater from an upstream source of glacial ice (Boulton and Deynoux, 1981). This facies may indicate deposition in a subaerial or subaqueous environment, but importantly, clast orientation distinguishes proglacial outwash from subglacial till (Boulton and Deynoux, 1981). The deposits may also exhibit normal grading and/or sedimentary structures indicative of soft-sediment deformation (e.g., loading structures, flame structures, sediment deformation beneath clasts; Boulton and Deynoux, 1981). Glacial outwash recorded in British Columbia (Clague, 1975) and the forefield of Mýrdalsjökull ice cap in Iceland (Kjær et al., 2004) feature similar structures seen in several units among our Puget Lowland outcrop sites. Using the defined classification of glacial outwash, Units 1 and 2 from Fort Casey Site 1, Units 4 and 5 from Fort Casey Site 2, Units 1 and 5 from Penn Cove, and Units 1 and 3 from Cliffside are interpreted as glacial outwash deposits (Figures 1, 2).

A third diamicton, structurally similar to those interpreted as glacial till yet containing articulated and/or broken marine shells, occasional winnowing of fine-matrix material, and sedimentary structures such as wavy laminations, is interpreted as **glacimarine deposits,** composed of both glacial and pelagic sediments that accumulate on the ocean floor seward of the ice margin. Such pelagic sediments have been samples from a geographically-diverse population of sediment cores from deglaciated continental margins (e.g., Anderson et al., 1980; Prothro et al., 2018; Smith et al., 2019), although preservation of shells and other carbonate-based materials are less common in Antarctic glaciomarine sediments. Glacimarine deposits are also identified in coastal outcrop deposits of northern Svalbard with similar characteristics (Alexanderson et al., 2018). Both Unit 1 from Double Bluff and Unit 2 from Penn Cove are consistent with these classifications and closely resemble the structure and composition of the glacimarine deposits identified on deglaciated continental margins (Figures 1, 2; Anderson et al., 1980; Prothro et al., 2018). At sites Double Bluff and Penn Cove, this facies (a.k.a. Everson Glaciomarine Drift) overlays glacial till, indicating ice marginal retreat into a marine setting with sand-rich deposits recording removal of fines by bottom currents. Conversely, glacial till that stratigraphically transitions upsection into cross-bedded sands with parallel-to-bed oriented clasts and wavy laminations that are barren of marine shells indicate retreat into a subaerial environment, as is observed proximal to the Mýrdalsjökull ice cap in Iceland (Kjær et al., 2004). Unit 3 from West Beach Site 1 and Unit 5 from Cliffside record such evidence of **subaerial glacial retreat** both meet these classifications (Figures 1, 2).

Facies transitions where grain sizes coarsen-upward (a.k.a. reverse grading) and changes in MS values can be associated with **landscape emergence** and differentiation of source material, respectively (Komar, 1977; McCabe, 1986; Sengupta, 2017). Regardless of the process(es) explaining the observed grain coarsening, which may include relative sea level fall outpacing eustatic sea-level rise, tectonic activity, glacial isostatic response, or a combination of these factors, we would expect such processes to be marked by facies transitions along the coast. In the Puget Lowland, emergence above sea level has been recorded in the stratigraphy by thin subaerial deposits (e.g., fluvial sediments and soil) overlying the glacial and glaciomarine deposits (Domack, 1984; Demet et al., 2019). The preservation of the glacial till organization and sedimentary structures including cross-bedding features in the Puget Lowland indicate coarsening-upward seen in the sedimentary record is not a result of tectonic activity. Coarsening-upward grain sizes seen in the transition from finer marine sediments to coastal deposits have been identified in coastal outcrops in northern Svalbard and are interpreted to indicate relative sea level fall (McCabe, 1986; Alexanderson et al., 2018). While glacial isostatic rebound is not responsible for the shallowing-upward of Svalbard facies (Alexanderson et al., 2018), the facies and coarsening material identified between Units 3 and 2 at Fort Casey Site 2, transition from Unit 5 laminated silt to Unit 4 cross-bedded sand at Penn Cove, and coarsening of grain size with peaks and MS across Units 7 and 6 at West Beach Site 2 could be connected to land emergence events (Figures 1, 2).

Facies transitions where grain-sizes fine upward, correspond with increases or decreases in MS, and are accompanied by the appearance of marine shells are associated with **landscape submergence** (Sengupta, 2017; Komar, 1977). Similarly classified facies that mark the transition from a subaerial to a submarine environment have been seen in seismic profiles and regional stratigraphic data in the southwestern Pacific in South Island, New Zealand (Carter et al., 1986). Therefore, the fining of material between Unit 4 sand deposits to Unit 3 silts at Double Bluff, introduction of shells to the fining material between Units 2 and 1 at West Beach Site 1, and fining of grain size across the Unit 2 and 1 boundary at West Beach Site 2 are all interpreted as a transition to a submarine setting (Figures 1, 2).

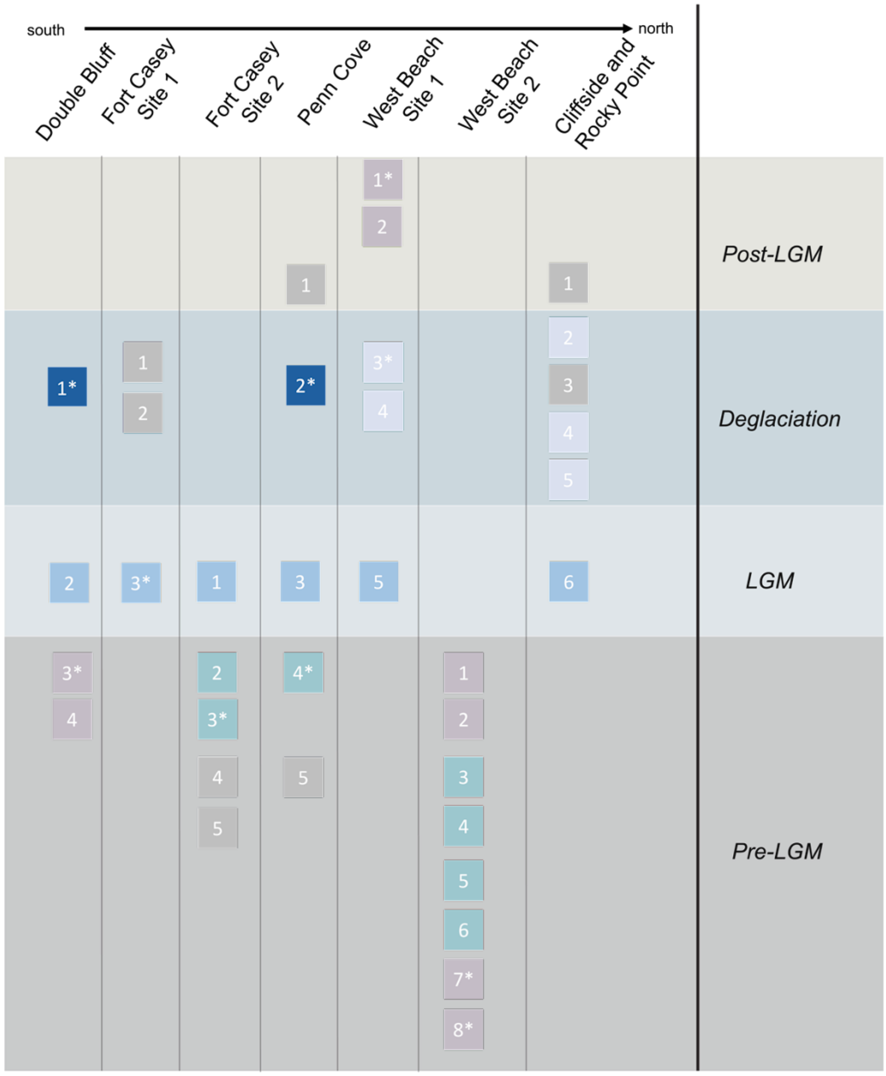


| Site | Unit | Type | Date (kya) |
|---|---|---|---|
| Double Bluff | 1,3 | | 48.0+ cal. BP |
| Fort Casey Site 1 | 3 | | 9.33 ± 2.3 |
| Fort Casey Site 2 | 3 | | 56.6 ± 15.5 ; 40.8 ± 8.2 |
| Penn Cove | 2 | | 12.9 ± 0.3 cal. BP; 12.1 ± 0.3 cal. BP |
| | 4 | | 56.6 ± 4.1 ; 44.4 ± 2.8 |
| West Beach Site 1 | 1 | | 1.56 ± 0.1 cal. BP |
| | 3 | | 6.2 ± 0.6 ; 4.1 ± 1.8 |
| West Beach Site 2 | 7 | | 30.7 ± 2.5 ; 29.2 ± 4.6 |
| | 8 | | 38.1 ± 9.7 ; 31.3 ± 2.65 |

= glacial till
= glacial outwash
= marine deglaciation
= subaerial deglaciation
=landscape emergence
=landscape submergence

**Figure 2.** Grouping of facies based on depositional time periods across Whidbey Island. Units with asterisks have radiocarbon or OSL dates included in the table on the lower left.

## 4.2 Pre-LGM landscape evolution

Prior to glacial advance of the Puget Lobe across Whidbey Island during the LGM, several submergence and emergence facies transitions record dynamic landscape changes. Landscape emergence above sea level prior to LGM glaciation is recorded by outcrops exposed at Penn Cove and Fort Casey Site 2. Penn Cove OSL ages identify this landscape emergence to occur between 56.6 ± 4.1 and 44.4 ± 2.8 kya. Similar Fort Casey Site 2 OSL ages constrain this transition to having occurred from 56.6 ± 15.5 to 40.8 ± 8.2 kya, placing the emergence within the MIS 4 glacial and MIS 3 interglacial stages, which may be connected to a lack of ice coverage and reduced CIS loading of the solid Earth at these times.

A sequence of submergent and emergent facies are observed in the pre-LGM deposits at West Beach Site 2. OSL dates places a submergence event between 38.1 ± 9.7 and 31.3 ± 2.65 kya while OSL dates from overlying facies places subsequent emergence between 30.7 ± 2.5 and 29.2 ± 4.6 kya. Both of these events occurred within the MIS 3 interglacial. This rapid transition between landscape submergence and emergence not only identifies high sedimentation rates at this site during MIS 3, but also suggests that the Puget Lowland experienced rapid landscape changes during MIS 3. Clay and sand deposits included as part of the emergence and submergence interpretation may have previously been identified and referred to as the Lawton Clay (Mullineaux et al., 1965) and Esperance Sands, respectively. Prior to LGM ice advance into the Strait of Juan de Fuca, the Puget Lowland was cut-off and developed into a proglacial lake basin, responsible for the deposition of the Lawton Clay (Mullineaux et al., 1965). Southward migrating proglacial channels deposited the Esperance Sands and developed into a large outwash plain across the Puget Lowland, radiocarbon dated to 18,000-20,000 years ago (Mullineaux et al., 1965; Crandell et al., 1966; Easterbrook, 1969; Clague, 1976; Booth, 1994). While the uncertainties in our OSL-dates contribute to discrepancy with previously collected radiocarbon dates of the Esperance Sands (Text S2; Easterbrook, 1969), the OSL ages relative to each other are useful in considering rates of sediment deposition and landscape evolution.

**4.3 LGM glacial advance**

Erosional contacts between glacial till (Vashon Till) and underlying facies mark LGM advance of the Puget Lobe into the region at multiple sites across Whidbey Island including Double Bluff, Fort Casey Site 2, and Penn Cove (Figure S2A). OSL ages from below the erosional contact of LGM tills places maximum age of ice extent at 56.6 ± 4.1 and 44.4 ± 2.8 kya, within the timeframe of MIS 5. However, previously radiocarbon dated-wood material more precisely dates final LGM advance into the region after 17,500 cal. yr. BP (Mullineaux et al., 1965; Porter & Swanson, 1998; Table 2). This major difference in ages suggests a great deal of glacial erosion at the ice-bed boundary of the Puget Lobe during ice advance.

**4.4 Deglaciation**

Glacimarine sediments (Everson Glaciomarine Drift) in the uppermost 50 cm of Double Bluff Unit 1 record retreat of the Puget Lobe within a marine environment (Figure S2B; Thorson, 1980; Dethier et al., 1995; Demet et al., 2019). At Penn Cove, the presence of articulated shells and winnowing of smaller grain sizes from glacial tills suggests ice retreat in a marine environment. Five articulated shells found at Penn Cove were radiocarbon dated to a range of dates between 12.9 ± 0.3 and 12.1 ± 0.3 kya cal. yr. BP (Table 1), placing glacial ice in this region for ~3,000 years longer than previously thought (e.g., Easterbrook, 1992; Dethier et al., 1995; Swanson & Caffee, 2001). Based on the range in shell radiocarbon dates, glacial ice also appears to have been stable at Penn Cove for at least 1,000 years (Figure 1A) with high sedimentation rates, accumulating 2.5 m during glaciation. Improved constraints on timing of Puget Lobe retreat has important implications for eustatic sea-level rise during the late Pleistocene and suggests Puget Lobe contributions to Meltwater Pulse 1A (Peltier, 2005; Gomez et al., 2015; Gorbarenko et al., 2019; Yokoyama & Purcell, 2021).

Deglacial facies seen at the more northern West Beach Site 1 and Cliffside indicate ice retreat within a subaerial environment (Figure S2A). The change in ice retreat style seen from the more southern Double Bluff and Penn Cove sites to the northern West Beach and Cliffside sites may be due to the substantial, 1,000-year stand-still of ice at Penn Cove. The duration of ice stability at this location is an indication that ice retreat was step-wise, rather than catastrophic (c.f., Easterbrook, 1992). Step-wise retreat of the ice margin is also supported by the presence of grounding-zone wedges (GZWs); the development of these ice-marginal landforms were likely supported by the identified high rates of sedimentation in the region (~2.5 mm/year; Simkins et al., 2017; Simkins et al., 2018; Demet et al., 2019). Additionally, the Rocky Point site features a bedrock high (i.e., a potential pinning point of ice; Hogan et al., 2020) and mapped GZWs, suggesting this site could have periodically stabilized ice during land rebound before final deglaciation of the region (Simkins et al., 2018; Demet et al., 2019).

### 4.5 Post-LGM landscape evolution

Following deglaciation of Whidbey Island, the Penn Cove and Cliffside sites record outwash deposits from proglacial fluvial sources. An OSL age within the submergence facies of Unit 2 at West Beach Site 1 marks the transition from a post-glacial fluvial environment to a submarine environment between 6.2 ± 0.6 and 4.1 ± 1.8 kya. Radiocarbon-dated shell hash sampled from the uppermost unit at this same West Beach Site 1 suggests a highly energetic aquatic marine or coastal environment was present in this location as early as 1.56 ± 0.1 kya cal. BP, at least 5,000 years following ice loss in the Puget Lowland. After initial lithospheric rebound from ice-loading and the possibility of a local tectonic event, it is feasible vertical land movement slowed enough to allow local sea level to resubmerge the region around 1,000 years ago (Figure 1A, 2). Overall, findings from this work support better understanding of the extinct CIS while also elucidating the role GIA and subglacial topography may play in determining ice-margin retreat styles for systems with similar subglacial topography and rheologic settings such as margins of Greenland and the Antarctic Peninsula (Eyles et al., 2018; Whitehouse et al., 2019; Nield et al., 2014).

## 5 Conclusions

This decimeter-scale physical sedimentological assessment, paired with geochronological assessment of seven sites across the deglaciated Puget Lowland, provides spatiotemporal information on landscape emergence and submergence as well as final ice advance and retreat of the southernmost CIS. Rates of vertical landscape changes constrained through OSL dating indicates the Puget Lowland was a highly dynamic region where a sequence of landscape emergence and submergence occurred within ~1,000 years during MIS 3 despite the concurrent period of rapid and substantial global mean sea level rise (Yokoyama & Purcell, 2021). Additionally, these findings place glacial ice in the Puget Lowland for 3,000 years longer during the LGM than previously thought, with final retreat occurring across the middle of Whidbey Island at approximately 12.1 ± 0.3 kya cal. BP, which may have implications for contributions to Meltwater Pulse 1A. Radiocarbon dates are used to show ice marginal stand-still and substantial grounding zone sedimentation during final retreat. While more southern sites (e.g., Double Bluff and Penn Cove) record ice retreat within submarine environments, the northernmost sites (e.g., Cliffside and Rocky Point), which feature a topographic high and previously mapped grounding-zone wedges (Demet et al., 2019), appear to record ice retreat into a subaerial environment. This data records empirical evidence of rapid vertical landscape evolution and paired marine-terminating ice stability for at least a millennium. The similarities between the rheology in this location and the rheology of the Antarctic Peninsula, as well as the topographic similarities between the Puget Lowland and modern margins of the Greenland Ice Sheet make these findings highly relevant to increasing process-based understanding of solid Earth influence on ice dynamics in contemporary marine-terminating glacial systems.

## Acknowledgments

The sites analyzed for this work are located on land historically cultivated and inhabited by the Skokomish, Suquamish, Squaxin, Stl'pulmsh, Steilacoom, Puyallup, Muckleshoot, and Duwamish peoples, while much of the data analysis and interpretation were conducted on land cultivated and inhabited by the Monacan Nation. The peoples of these Nations were custodians of the land for time immemorial before forced removal and genocide during colonization. The authors acknowledge their ongoing stewardship of the lands. This work was funded by the Chamberlain Endowment and the H.G. Goodell Endowment at the University of Virginia. The funding and support for the radiocarbon dates presented was made possible through the NOSAMS Graduate Student Internship at Woods Hole Institute, supported by NSF cooperative agreement OCE-1755125, and the Burke Institute. Thank you to Dr. Mark Kurz, Dr. Roberta Hansman, Anne Cruz, Mary Lardie Gaylord, and Nan Trowbridge for their hospitality and guidance throughout M. McKenzie's internship. The authors declare that they have no conflict of interest.

## Open Research

Digital data including site coordinates and sample grain size, trace element (not included in analysis), moisture content, and magnetic susceptibility data and all 236 physical samples are housed in the PANGAEA database (McKenzie et al., *submitted*) and at the Washington Department of Natural Resources at the Washington Geological Survey. Physical samples are in WhirlPak bags, labelled by site name, number, and sampling interval in centimeters. When collected in the field, unit names were given from down-to-up outcrop. For the purpose of simplicity, the unit names were flipped for manuscript analyses to be listed as smallest to highest up-to-down outcrop. To request physical data, please contact Jessica Czajkowski (Jessica.Czajkowski@dnr.wa.gov) and/or Ashley Cabibbo (Ashley.Cabibbo@dnr.wa.gov) at the Washington State Department of Natural Resources.

## References


Alexanderson, H., Henriksen, M., Ryen, H.T., Landvik, J.Y., & Peterson, G. (2018). 200 ka of glacial events in NW Svalbard: an emergence cycle facies model and regional correlations. *Arktos, 4*, 1-25. https://doi.org/10.1007/s41063-018-0037-z

Alley, R. B., Holschuh, N., MacAyeal, D. R., Parizek, B. R., Zoet, L., Riverman, K., Muto, A., Christianson, K., Clyne, E., Anandakrishnan, S., Stevens, N., & GHOST Collaboration. (2021). Bedforms of Thwaites Glacier, West Antarctica: Character and Origin. *Journal of Geophysical Research: Earth Surface*, *126*(12). https://doi.org/10.1029/2021JF006339

Anderson, J.B., Kurtz, D.D., Domack, E.W., & Balshaw, K.M. (1980). Glacial and Glacial Marine Sediments of the Antarctic Continental Shelf. *The Journal of Geology*. 88(4). https://www.journals.uchicago.edu/doi/pdf/10.1086/628524

Anundsen, K., Abella, S., Leopold, E., Stuiver, M., & Turner, S. (1994). Late-Glacial and Early Holocene Sea-Level Fluctuations in the Central Puget Lowland, Washington, Inferred from Lake Sediments. *Quaternary Research*, *42*(2), 149–161. https://doi.org/10.1006/qres.1994.1064

Armstrong, J.E., Crandell, D.R., Easterbrook, D.J., & Noble, J.B. (1965). Late Pleistocene Stratigraphy and Chronology in Southwestern British Columbia and Northwestern Washington. Geological Society of America, 76(3), 321-330.

Auclair, M., Lamothe, M., & Huot, S. (2003). Measurement of anomalous fading for feldspar IRSL using SAR. *Radiation Measurements*, *37*(4), 487–492. https://doi.org/10.1016/S1350-4487(03)00018-0

Barbouti, A. I., & Rastin, B. C. (1983). A study of the absolute intensity of muons at sea level and under various thicknesses of absorber. *Journal of Physics G: Nuclear Physics*, *9*(12), 1577. https://doi.org/10.1088/0305-4616/9/12/018

Booth, D. B. (1987). Timing and processes of deglaciation along the southern margin of the Cordilleran ice sheet. In W. F. Ruddiman & H. E. Wright (Eds.), *North America and Adjacent Oceans During the Last Deglaciation* (pp. 71–90). Geological Society of America. https://doi.org/10.1130/DNAG-GNA-K3.71

Booth, D. B., & Hallet, B. (1993). Channel networks carved by subglacial water: Observations and reconstruction in the eastern Puget Lowland of Washington. *Geological Society of America Bulletin*, *105*(5), 671–683. https://doi.org/10.1130/0016-7606(1993)105<0671:CNCBSW>2.3.CO;2

Booth, D. (1994). Glaciofluvial infilling and scour of the Puget Lowland, Washington, during ice sheet glaciation. Geology, 22, 695-698.

Booth, D. B., Troost, K. G., Clague, J. J., & Waitt, R. B. (2003). The Cordilleran Ice Sheet. In *Developments in Quaternary Sciences* (Vol. 1, pp. 17–43). Elsevier. https://doi.org/10.1016/S1571-0866(03)01002-9

Bøtter-Jensen, L., & Murray, A. S. (1999). Developments in Optically Stimulated Luminescence Techniques for Dating and Retrospective Dosimetry. *Radiation Protection Dosimetry*, *84*(1), 307–315. https://doi.org/10.1093/oxfordjournals.rpd.a032745

Boulton, G. S., & Deynoux, M. (1981). Sedimentation in glacial environments and the identification of tills and tillites in ancient sedimentary sequences. *Precambrian Research*, *15*(3–4), 397–422. https://doi.org/10.1016/0301-9268(81)90059-0

Carter, R.M., Carter, L., & Johnson, D.P. (1986). Submergent shorelines in the SW Pacific: evidence for an episodic post-glacial transgression. *Sedimentology*, *33*(5), 629-649. https://doi.org/10.1111/j.1365-3091.1986.tb01967.x

Clague, J. J. (1975). Sedimentology and paleohydrology of late Wisconsinan outwash, Rocky Mountain trench, southeastern British Columbia. *Glaciofluvial and Glaciolacustrine Sedimentation.*

Clague, J.J. (1976). Quadra Sand and its relation to the late Wisconsin glaciation of southwest British Columbia. Canadian Journal of Earth Sciences, 13(6), 717-875.

Clague, J. J. (1981). Late Quaternary geology and geochronology of British Columbia, Part 2. Geological Survey of Canada, 80-35, 41.

Clark, P. U. (1994). Unstable Behavior of the Laurentide Ice Sheet over Deforming Sediment and Its Implications for Climate Change. *Quaternary Research*, *41*(1), 19–25. https://doi.org/10.1006/qres.1994.1002

Clarke, G. K. C., Nitsan, U., & Paterson, W. S. B. (1977). Strain heating and creep instability in glaciers and ice sheets. *Reviews of Geophysics*, *15*(2), 235. https://doi.org/10.1029/RG015i002p00235

Crandell, D.R., Mullineaux, D.R., & Waldron, H.H. (1966). Age and origin of the Puget Sound trough in western Washington. U.S. Geological Survey, 525-B, B132-B136.

Cuffey, K., & Paterson, W. S. B. (2010). *The physics of glaciers* (4th ed). Butterworth-Heinemann/Elsevier.

Demet, B. P., Nittrouer, J. A., Anderson, J. B., & Simkins, L. M. (2019). Sedimentary processes at ice sheet grounding-zone wedges revealed by outcrops, Washington State (USA). *Earth Surface Processes and Landforms*, *44*(6), 1209–1220. https://doi.org/10.1002/esp.4550

Dethier, D. P., Pessl, F., Keuler, R. F., Balzarini, M. A., & Pevear, D. R. (1995). Late Wisconsinan glaciomarine deposition and isostatic rebound, northern Puget Lowland, Washington. *Geological Society of America Bulletin*, *107*(11), 1288–1303. https://doi.org/10.1130/0016-7606(1995)107<1288:LWGDAI>2.3.CO;2

Domack, E.W. (1984). Rhythmically Bedded Glaciomarine Sediments on Whidbey Island, Washington. *SEPM Journal of Sedimentary Research*, *Vol. 54*. https://doi.org/10.1306/212F847C-2B24-11D7-8648000102C1865D

Domack, E.W. (1983). Facies of late Pleistocene glacial-marine sediments on Whidbey Island, Washington: An isostatic glacial-marine sequence in Molnia, B.F. (ed.) Glacial-Marine Sedimentation: Plenum, New York, 535-570.

Duller G.A.T. (2013). Luminescence Analyst, 4.11 ed, Aberystwyth University.

Duller, G.A.T. (2015). Luminescence dating. In W.J. Rink, & J.W. Thompson (Eds.), Encyclopedia of Scientific Dating Methods (pp. 390-404). (Encyclopedia of Earth Science Series). Springer Nature.

Durand, G., Gagliardini, O., Favier, L., Zwinger, T., & Le Meur, E. (2011). Impact of bedrock description on modeling ice sheet dynamics: BEDROCK DESCRIPTION TO MODEL ICE SHEET. *Geophysical Research Letters*, *38*(20), n/a-n/a.

Easterbrook, D. J. (1992). Advance and Retreat of Cordilleran Ice Sheets in Washington, U.S.A. *Géographie Physique et Quaternaire*, *46*(1), 51–68. https://doi.org/10.7202/032888ar

Easterbrook, D.J., Crandell, D.R., & Leopold, E.B. (1967). Pre-Olympia Pleistocene stratigraphy and chronology in the central Puget Lowland, Washington. Geological Society of America Bulletin, 78(1), 13-20.

Easterbrook, D. (1969). Pleistocene Chronology of the Puget Lowland and San Juan Islands, Washington. Geological Society of America Bulletin, 80, 2273-2286.

Easterbrook, D.J. (1986). Stratigraphy and chronology of Quaternary deposits of the Puget Lowland and Olympic Mountains of Washington and the Cascade Mountains of Washington and Oregon. Quaternary Science Reviews, 5, 145-159.

Evans, D.J.A., & Thompson, S.A. (2010) Glacial sediments and landforms of Holderness, eastern England: A glacial depositional model for the North Sea Lobe of the British-Irish Ice Sheet. *Earth-Science Reviews* 101(3-4), p. 147-189. https://doi.org/10.1016/j.earscirev.2010.04.003

Eyles, N., Arbelaez Moreno, L., & Sookhan, S. (2018). Ice streams of the Late Wisconsin Cordilleran Ice Sheet in western North America. *Quaternary Science Reviews*, *179*, 87–122. https://doi.org/10.1016/j.quascirev.2017.10.027

Favier, L., Pattyn, F., Berger, S., & Drews, R. (2016). Dynamic influence of pinning points on marine ice-sheet stability: a numerical study in Dronning Maud Land, East Antarctica. *The Cryosphere*, *10*(6), 2623–2635. https://doi.org/10.5194/tc-10-2623-2016

Galbraith, R. F., Roberts, R. G., Laslett, G. M., Yoshida, H., & Olley, J. M. (1999). Optical dating of single and multiple grains of quartz from Jinmium rock shelter, Northern Australia: Prt 1, Experimental design and statistical models. *Archaeometry*, *41*(2), 339–364. https://doi.org/10.1111/j.1475-4754.1999.tb00987.x

Goebel, T. Waters, M., & O'rourke, D. (2011). The Late Pleistocene Dispersal of Modern Humans in the Americas. Science, 319, 1497.

Goehring, B. M., Wilson, J., & Nichols, K. (2019). A fully automated system for the extraction of in situ cosmogenic carbon-14 in the Tulane University cosmogenic nuclide laboratory. *Nuclear Instruments and Methods in Physics Research Section B: Beam Interactions with Materials and Atoms*, *455*, 284–292. https://doi.org/10.1016/j.nimb.2019.02.006

Gomez, N., Gregoire, L. J., Mitrovica, J. X., & Payne, A. J. (2015). Laurentide-Cordilleran Ice Sheet saddle collapse as a contribution to meltwater pulse 1A. *Geophysical Research Letters*, *42*(10), 3954-3962. **https://doi.org/10.1002/2015GL063960**

Gorbarenko, S., Shi, X., Zou, J., Velivetskaya, T., Artemova, A., Liu, Y., Yanchenko, E. & Vasilenko, Y. (2019). Evidence of meltwater pulses into the North Pacific over the last 20 ka due to the decay of Kamchatka Glaciers and Cordilleran Ice Sheet. *Global and Planetary Change*, *172*, 33-44. https://doi.org/10.1016/j.gloplacha.2018.09.014

Guérin, G., Mercier, N., Adamiec, G., (2011). Dose-rate conversion factors: update. *Ancient TL 29(1)*, 5-8.

Hatfield, R. G., Stoner, J. S., Reilly, B. T., Tepley, F. J., Wheeler, B. H., & Housen, B. A. (2017). Grain size dependent magnetic discrimination of Iceland and South Greenland terrestrial sediments in the northern North Atlantic sediment record. *Earth and Planetary Science Letters*, *474*, 474–489. https://doi.org/10.1016/j.epsl.2017.06.042

Heaton, T. J., Köhler, P., Butzin, M., Bard, E., Reimer, R. W., Austin, W. E. N., Bronk Ramsey, C., Grootes, P. M., Hughen, K. A., Kromer, B., Reimer, P. J., Adkins, J., Burke, A., Cook, M. S., Olsen, J., & Skinner, L. C. (2020). Marine20—The Marine Radiocarbon Age Calibration Curve (0–55,000 cal BP). *Radiocarbon*, *62*(4), 779–820. https://doi.org/10.1017/RDC.2020.68

Hogan, K.A., Larter, R.D., Graham, A.G.C., Arthern, R., Kirkham, J.D., Totten, R.L., Jordan, T.A., Clark, R., Fitzgerald, V., Wåhlin,A.K., Anderson, J.B., Hillenbrand, C., Nitsche, F.O., Simkins, L., Smith, J.A., Gohl, K., Arndt, J.E., Hong, J., & Wellner, J. (2020). Revealing the former bed of Thwaites Glacier using sea-floor bathymetry:implications for warm-water routing and bed controls on ice flow and buttressing. *The Cryosphere* 14(9), p. 2883-2908. https://doi.org/10.5194/tc-14-2883-2020

Jamieson, S. S. R., Vieli, A., Livingstone, S. J., Cofaigh, C. Ó., Stokes, C., Hillenbrand, C.-D., & Dowdeswell, J. A. (2012). Ice-stream stability on a reverse bed slope. *Nature Geoscience, 5*(11), 799–802. https://doi.org/10.1038/ngeo1600

King, G. E., Robinson, R. A. J., & Finch, A. A. (2014). Towards successful OSL sampling strategies in glacial environments: deciphering the influence of depositional processes on bleaching of modern glacial sediments from Jostedalen, Southern Norway. *Quaternary Science Reviews*, *89*, 94–107. https://doi.org/10.1016/j.quascirev.2014.02.001

Kirshner, A. E., Anderson, J. B., Jakobsson, M., O'Regan, M., Majewski, W., & Nitsche, F. O. (2012). Post-LGM deglaciation in Pine island Bay, west Antarctica. *Quaternary Science Reviews*, *38*, 11-26. https://doi.org/10.1016/j.quascirev.2012.01.017

Kjær, K.H., Sultan, L., Krüger, J., & Schomacker, A. (2004). Architecture and sedimentation of outwash fans in front of the Mýrdalsjökull ice cap, Iceland. *Sedimentary Geology, 172*(1-2), 139-163. https://doi.org/10.1016/j.sedgeo.2004.08.002.

Komar, P. (1977). BEACH PROCESSES AND SEDIMENTATION. *Beach Processes and Sedimentation.*

Kovanen, D. J., & Slaymaker, O. (2004). Relict Shorelines and Ice Flow Patterns of the Northern Puget Lowland from Lidar Data and Digital Terrain Modelling. *Geografiska Annaler. Series A, Physical Geography*, *86*(4), 385–400. https://www.jstor.org/stable/3566155

Leopold, E. B., Nickmann, R., Hedges, J. I., & Ertel, J. R. (1982). Pollen and Lignin Records of Late Quaternary Vegetation, Lake Washington. *Science*, *218*(4579), 1305–1307. https://doi.org/10.1126/science.218.4579.1305

Lesnek, A. J., Briner, J. P., Lindqvist, C., Baichtal, J. F., & Heaton, T. H. (2018). Deglaciation of the Pacific coastal corridor directly preceded the human colonization of the Americas. *Science Advances*, *4*(5), eaar5040. https://doi.org/10.1126/sciadv.aar5040

Mandryk, C. A. S., Josenhans, H., Fedje, D. W., & Mathewes, R. W. (2001). Late Quaternary paleoenvironments of Northwestern North America: implications for inland versus coastal migration routes. *Quaternary Science Reviews*, *20*(1), 301–314. https://doi.org/10.1016/S0277-3791(00)00115-3

Margold, M., Stokes, C. R., & Clark, C. D. (2015). Ice streams in the Laurentide Ice Sheet: Identification, characteristics and comparison to modern ice sheets. *Earth-Science Reviews*, *143*, 117–146. https://doi.org/10.1016/j.earscirev.2015.01.011

McCabe, A.M. (1986). Glaciomarine facies deposited by retreating tidewater glaciers; an example from the late Pleistocene of Northern Ireland. *Journal of Sedimentary Research*. 56 (6): 880–894. doi: https://doi.org/10.1306/212F8A76-2B24-11D7-8648000102C1865D

McKenzie, M. A., Miller, L. E., Lepp, A. P., & DeWitt, R. (*submitted*) Physical and chemical sedimentology conducted on coastal outcrops across Whidbey Island, Washington state. PANGAEA Data Archiving & Publication (PDI-36347).

McKenzie, M. A., Miller, L. E., Slawson, J. S., MacKie, E. J., & Wang, S. (2023). Differential impact of isolated topographic bumps on ice sheet flow and subglacial processes. *The Cryosphere*, *17*(6), 2477-2486. https://doi.org/10.5194/tc-17-2477-2023

Menounos, B., Goehring, B.M., Osborn, G., Margold, M., Ward, B., Bond, J., … & Heyman, J. (2017). Cordilleran Ice Sheet mass loss preceded climate reversals near the Pleistocene Termination. *Science, 358*(6364), 781-784.

Mullineaux, D.R., Waldron, H.H., & Rubin, M. (1965). Stratigraphy and chronology of late interglacial and early Vashon time in the Seattle area, Washington. U.S. Geological Survey Bulletin, 1194-O, 10.

Murray, A. S., & Wintle, A. G. (2000). Luminescence dating of quartz using an improved single-aliquot regenerative-dose protocol. *Radiation Measurements*, *32*(1), 57–73. https://doi.org/10.1016/S1350-4487(99)00253-X

Nield, G. A., Barletta, V. R., Bordoni, A., King, M. A., Whitehouse, P. L., Clarke, P. J., Domack, E., Scambos, T. A., & Berthier, E. (2014). Rapid bedrock uplift in the Antarctic Peninsula explained by viscoelastic response to recent ice unloading. *Earth and Planetary Science Letters*, *397*, 32–41. https://doi.org/10.1016/j.epsl.2014.04.019

O'Regan, M., Cronin, T. M., Reilly, B., Alstrup, A. K. O., Gemery, L., Golub, A., ... & Jakobsson, M. (2021). The Holocene dynamics of Ryder Glacier and ice tongue in north Greenland. *The Cryosphere*, *15*(8), 4073-4097. https://doi.org/10.5194/tc-15-4073-2021

Peltier, W.R. (2005). On the hemispheric origins of meltwater pulse 1a. *Quaternary Science Reviews.* 24(14-15) p. 1655-1671. https://doi.org/10/1016/j.quascirev.2004.06.023

Pessl Jr., F., Dethier, D.P., Keuler, R.F., Minard, J.P., & Balzarini, M.A. (1981). Sedimentary facies and depositional environments of late Wisconsin glacial-marine deposits in the central Puget Lowland, Washington. American Association Petroleum Geologists, Abstracts, Arm. Meeting, San Francisco.

Polenz, M., Slaughter, S. L., & Thorsen, G. W. (2005). Geologic map of the Coupeville and part of the Port Townsend North 7.5-minute quadrangles, Island County, Washington. Washington Division of Geology and Earth Resources Geologic Map, GM-58, 1 sheet, scale 1: 24,000.

Porter, S. C., & Swanson, T. W. (1998). Radiocarbon Age Constraints on Rates of Advance and Retreat of the Puget Lobe of the Cordilleran Ice Sheet during the Last Glaciation. *Quaternary Research*, *50*(3), 205–213. https://doi.org/10.1006/qres.1998.2004

Powell, R.D. (1980). Holocene glacimarine deposition by tide-water glaciers in Glacier Bay, Alaska [unpublished Ph.D. thesis]. Ohio State University.

Prescott, J. R., Stephan, L. G. (1982). The contribution of cosmic radiation to the environmental dose for thermoluminescence dating. *PACT*, *6*, 17–25. https://cir.nii.ac.jp/crid/1573668924373277824

Prescott, J. R., & Hutton, J. T. (1994). Cosmic ray contributions to dose rates for luminescence and ESR dating: Large depths and long-term time variations. *Radiation Measurements*, *23*(2), 497–500. https://doi.org/10.1016/1350-4487(94)90086-8

Prothro, L.O., Simkins, L.M., Majewski, W., & Anderson, J.B. (2018). Glacial retreat patterns and processes determined from integrated sedimentology and geomorphology records. Marine Geology, 395, 104-119.

Reilly, B. T., Stoner, J. S., Mix, A. C., Walczak, M. H., Jennings, A., Jakobsson, M., Dyke, L., Glueder, A., Nicholls, K., Hogan, K. A., Mayer, L. A., Hatfield, R. G., Albert, S., Marcott, S., Fallon, S., & Cheseby, M. (2019). Holocene break-up and reestablishment of the Petermann Ice Tongue, Northwest Greenland. *Quaternary Science Reviews*, *218*, 322–342. https://doi.org/10.1016/j.quascirev.2019.06.023

Rhodes, E. J. (2011). Optically Stimulated Luminescence Dating of Sediments over the Past 200,000 Years. *Annual Review of Earth and Planetary Sciences*, *39*(1), 461–488. https://doi.org/10.1146/annurev-earth-040610-133425

Rigg, G. B., & Gould, H. R. (1957). Age of Glacier Peak eruption and chronology of post-glacial peat deposits in Washington and surrounding areas. *American Journal of Science*, *255*(5), 341–363. https://doi.org/10.2475/ajs.255.5.341

Robel, A. A., Pegler, S. S., Catania, G., Felikson, D., & Simkins, L. M. (2022). Ambiguous stability of glaciers at bed peaks. *Journal of Glaciology*, *68*(272), 1177–1184. https://doi.org/10.1017/jog.2022.31

Roberts, M. L., Elder, K. L., Jenkins, W. J., Gagnon, A. R., Xu, L., Hlavenka, J. D., & Longworth, B. E. (2019). $^{14}$C Blank Corrections for 25–100 μg Samples at the National Ocean Sciences AMS Laboratory. *Radiocarbon*, *61*(5), 1403–1411. https://doi.org/10.1017/RDC.2019.74

Rosenbaum, J. G. (2005). Magnetic properties of sediments in cores BL96-1,-2, and-3 from Bear Lake, Utah and Idaho. *US Geological Survey Open-File Report*, (1203), 13p.

Sengupta, S. (2017). *Introduction to Sedimentology* (1st ed.). Routledge. https://doi.org/10.1201/9780203749883

Sheldon, C., Jennings, A., Andrews, J.T., Ó Cofaigh, C., Hogan, K., Dowdeswell, J.A., & Seidenkrantz, M. (2016). Ice stream retreat following the LGM and onset of the west Greenland current in Uummannaq Trough, west Greenland. *Quaternary Science Reviews*, 147, p. 27-46. https://goi.org/10.1016/j.quascirev.2016.01.019

Sherrod, B. L., Blakely, R. J., Weaver, C. S., Kelsey, H. M., Barnett, E., Liberty, L., Meagher, K. L., & Pape, K. (2008). Finding concealed active faults: Extending the southern Whidbey Island fault across the Puget Lowland, Washington. *Journal of Geophysical Research*, *113*(B5), B05313. https://doi.org/10.1029/2007JB005060

Shugar, D. H., Walker, I. J., Lian, O. B., Eamer, J. B. R., Neudorf, C., McLaren, D., & Fedje, D. (2014). Post-glacial sea-level change along the Pacific coast of North America. *Quaternary Science Reviews*, *97*, 170–192. https://doi.org/10.1016/j.quascirev.2014.05.022

Simkins, L. M., Anderson, J. B., & Demet, B. P. (2017). Grounding line processes of the southern Cordilleran Ice Sheet in the Puget Lowland. In R. A. Haugerud & H. M. Kelsey, *From the Puget Lowland to East of the Cascade Range<subtitle>Geologic Excursions in the Pacific Northwest</subtitle>*. Geological Society of America. https://doi.org/10.1130/2017.0049(03)

Simkins, L. M., Greenwood, S. L., & Anderson, J. B. (2018). Diagnosing ice sheet grounding line stability from landform morphology. *The Cryosphere*, *12*(8), 2707–2726. https://doi.org/10.5194/tc-12-2707-2018

Smith, J.A., Graham, A.G.C., Post, A.L. Hillenbrand, C., Bart, P. J., & Powell, R.D. (2019). The marine geological imprint of Antarctic ice shelves. *Nat Commun* **10**, 5635 (2019). https://doi.org/10.1038/s41467-019-13496-5

Stuiver, M., & Polach, H. A. (1977). Discussion reporting of 14C data. *Radiocarbon*, *19*(3), 355-363. https://doi.org/10.1017/S0033822200003672

Stuiver, M. (1980). Workshop On $^{14}$C Data Reporting. *Radiocarbon*, *22*(3), 964–966. https://doi.org/10.1017/S0033822200010389

Swanson, T. W., & Caffee, M. L. (2001). Determination of 36Cl Production Rates Derived from the Well-Dated Deglaciation Surfaces of Whidbey and Fidalgo Islands, Washington. *Quaternary Research*, *56*(3), 366–382. https://doi.org/10.1006/qres.2001.2278

Thompson, R., & Oldfield, F. (1986). *Environmental Magnetism*. London, Allen & Unwin.

Thorson, R. M. (1980). Ice-Sheet Glaciation of the Puget Lowland, Washington, during the Vashon Stade (Late Pleistocene)1. *Quaternary Research*, *13*(3), 303–321. https://doi.org/10.1016/0033-5894(80)90059-9

Thorson, R.M. (1981). Isostatic effects of the last glaciation in the Puget lowland, Washington. U.S. Geological Survey Open-File Report, 81-370, 100.

Thorson, R. (1989). Glacio-isostatic response of the Puget Sound area, Washington. Geological Society of America Bulletin, 101, 1163-1174.

van der Wal, W., Whitehouse, P. L., & Schrama, E. J. (2015). Effect of GIA models with 3D composite mantle viscosity on GRACE mass balance estimates for Antarctica. *Earth and Planetary Science Letters*, *414*, 134-143. https://doi.org/10.1016/j.epsl.2015.01.001

Verosub, K. L., & Roberts, A. P. (1995). Environmental magnetism: Past, present, and future. *Journal of Geophysical Research: Solid Earth*, *100*(B2), 2175–2192. https://doi.org/10.1029/94JB02713

Waitt Jr., R.B., & Thorson, R.M. (1983). The Cordilleran ice sheet is Washington, Idaho, and Montana. Late-quaternary environments of the United State, 1, 53-70.

Wallinga, J., & Cunningham, A. C. (2015). Luminescence dating, uncertainties and age range. *Encyclopedia of Scientific Dating Methods*, 440–445. https://doi.org/10.1007/978-94-007-6304-3_197

Wallinga, J., S. Murray, A., & B tter-Jensen, L. (2002). Measurement of the Dose in Quartz in the Presence of Feldspar Contamination. *Radiation Protection Dosimetry*, *101*(1), 367–370. https://doi.org/10.1093/oxfordjournals.rpd.a006003

Wan, J. X. W., Gomez, N., Latychev, K., & Han, H. K. (2022). Resolving glacial isostatic adjustment (GIA) in response to modern and future ice loss at marine grounding lines in West Antarctica. *The Cryosphere*, *16*(6), 2203-2223. https://doi.org/10.5194/tc-16-2203-2022

Weertman, J. (1974). Stability of the Junction of an Ice Sheet and an Ice Shelf. *Journal of Glaciology*, *13*(67), 3–11. https://doi.org/10.3189/S0022143000023327

Whillans, I. M., & Van Der Veen, C. J. (1997). The role of lateral drag in the dynamics of Ice Stream B, Antarctica. *Journal of Glaciology*, *43*(144), 231–237. https://doi.org/10.3189/S0022143000003178

Whitehouse, P. L., Gomez, N., King, M. A., & Wiens, D. A. (2019). Solid Earth change and the evolution of the Antarctic Ice Sheet. *Nature Communications*, *10*(1), 503. https://doi.org/10.1038/s41467-018-08068-y

Whitehouse, P.L. (2018). Glacial isostatic adjustment modelling: historical perspectives, recent advances, and future directions. *Earth Surface Dynamics, 6*, 401-429. https://doi.org/10.5194/esurf-6-401-2018.

Willis, B. (1898). Drift phenomena of Puget Sound. Geological Society of America Bulletin, 9, 111-16

Wintle, A. G., & Murray, A. S. (2006). A review of quartz optically stimulated luminescence characteristics and their relevance in single-aliquot regeneration dating protocols. *Radiation Measurements*, *41*(4), 369–391. https://doi.org/10.1016/j.radmeas.2005.11.001

Wintle AG. (1973). Anomalous fading of thermoluminescence in mineral samples. Nature 245:143–44

Yokoyama, Y., & Purcell, A. (2021). On the geophysical processes impacting palaeo-sea-level observations. *Geoscience Letters*, *8*(1), 13. https://doi.org/10.1186/s40562-021-00184-w

*Journal of Geophysical Research*

Supporting Information for

**Evidence of solid Earth influence on stability of the marine-terminating Puget Lobe of the Cordilleran Ice Sheet**

Marion A. McKenzie[1*], Lauren E. Miller[1], Allison P. Lepp[1], and Regina DeWitt[2]

[1]Department of Environmental Sciences, University of Virginia, 291 McCormick Rd., Charlottesville, VA, USA 22904
[2]Department of Physics, East Carolina University, 1000 E. 5th St., Greenville, NC, USA 27858-4353

Corresponding author: Marion McKenzie (marion.mckenzie@mines.edu)

[*]Author now affiliated with the Geology and Geological Engineering Department, Colorado School of Mines, 1105 Illinois St., Golden, CO, USA 80201

**Contents of this file**



**Introduction**

The contents here within contain additional text on historic studies of Puget Lowland outcrop units (Text S1) and sample collection, preparation, and age determination of optically stimulated luminescence samples (Text S2). The results of the OSL data are less reliable than those of the radiocarbon dates. We lack nuclide information for adjacent layers of OSL taken on unit boundaries and faced feldspar contamination in samples. While there is some partial disagreement between radiocarbon and OSL dates, the OSL dates are still highly useful in providing approximate rates of landscape evolution based on bracketed ages of landscape emergence and submergence (Figure 2).

Figure S1 exemplifies the difference between lenses and laminations identified in the field. Figure S2 depicts a schematic of glacial retreat within a marine environment versus glacial retreat within a subaerial environment.

Table S1 is a compilation of site information and sample types collected. Table S2 is the OSL measurement sequence used for age determination.

---

**Text S1.** Over the last six decades, this region has been studied with multiple approaches, varying resolutions, and differing classification methods. Therefore, to provide continuity between our analysis and prior work on final glacial-ice occupation and post-glacial landscape evolution in the Puget Lowland, we provide a summary of stratigraphic units thought to record pre-LGM, LGM, and post-LGM deglaciation and landscape evolution.

**S1.1** Pre-LGM and LGM deposits

A characteristic pre-LGM deposit in the Puget Lowland is the Lawton Clay, formed as the more southern Puget Lowland became a proglacial lake basin from ice advancement into the northern Strait of Juan de Fuca (Mullineaux et al., 1965; Figure 1B). Southward migrating proglacial channels that were active 18,000-20,000 years ago formed extensive outwash plain deposits referred to as the Esperance Sands and mark the oncoming advance of the CIS in the Puget Lowland (Mullineaux et al., 1965; Crandell et al., 1966; Easterbrook, 1969; Clague, 1976; Booth, 1994). The final stage of ice sheet advance during late-stage MIS 2 in the Puget Lobe is known as the Fraser glaciation and is marked by the deposition of the massive diamicton called the Vashon Till (Willis, 1898; Easterbrook, 1969; Clague, 1981; Domack, 1983; Easterbrook, 1986). Previously radiocarbon dated-wood collected beneath the Vashon Till provides a maximum age for the timing of final ice advance to the latitude of around Seattle (47.608013°N) at ~14,500 $^{14}$C years BP (~17,500 calendar years BP; Mullineaux et al., 1965; Porter & Swanson, 1998), although timing of maximum ice extent near Olympia, Washington (47.037872°N) is unknown and the degree of subglacial reworking and erosion of underlying strata is not well understood.

**S1.2** Deglacial and post-glacial deposits

Overlaying the Vashon Till in some locations in the Puget Lowland is the shell-bearing Everson Glaciomarine Drift deposits (Armstrong et al., 1965; Easterbrook, 1969; Powell, 1980; Thorson, 1980; Pessl et al., 1981; Domack, 1983, 1984; Dethier et al., 1995), marking the Puget Lobe as primarily grounded below sea level (Thorson, 1980; Dethier et al., 1995; Demet et al., 2019). The oldest marine shells dated from the Everson Glaciomarine Drift suggest the Puget Lowland was deglaciated and open to marine influence by 13,500 $^{14}$C years BP (~16,500 calendar years BP; Easterbook, 1992; Dethier et al., 1995; Swanson & Caffee, 2001). The lack of both sufficiently documented stratigraphic context for individual ages and a lack of marine reservoir correction for this region, however, contribute to uncertainties in this generalized date of deglaciation in the Puget Lowland (c.f., Porter & Swanson, 1998). Additionally, conflicting ages from freshwater lacustrine organics on the eastern fringe of the Puget Lowland suggest ice retreat before ~13,600 $^{14}$C years BP (~16,500 calendar years BP; Rigg & Gould, 1957; Leopold et al., 1982; Anundsen et al., 1994), and numerous cosmogenic exposure ages consistently indicate that retreat occurred ~15,500 years ago (Swanson & Caffee, 2001), while much of the CIS also experienced Pleistocene Termination mass loss before significant climate reversals (Menounos et al., 2017).

The presence of the Everson Glaciomarine Drift has been used to suggest a marine incursion beneath the Puget Lobe (Dethier et al., 1995; Swanson & Caffee, 2001), inciting a rapid lift-off of grounded ice (i.e., rapid transition from grounded ice to a floating ice shelf) of the southernmost CIS (Thorson, 1980, 1981; Waitt & Thorson, 1983; Booth, 1987; Booth et al., 2003). Synchronous retreat of the Puget Lobe and the largely westward flowing Juan de Fuca Lobe due to the decoupling of the Puget Lobe from its bed due to marine incursion has also been suggested (Easterbrook, 1992). However, major differences in deglacial stratigraphy across the Puget Lowland (Powell, 1980; Pessl et al., 1981; Domack, 1984; Demet et al., 2019), indicate variable patterns of retreat in time and space. Additionally, modern elevation of marine limits in the Puget Lowland, range from ~125 m above sea level in the northern San Juan islands to less than 30 m at the southern end of Whidbey Island (Thorson, 1981, 1989; Dethier et al., 1995; Kovanen & Slaymaker, 2004; Polenz et al., 2005), which indicates highly variable rates of GIA across the region. Emergence of this landscape from below to above sea level is distinctly marked in post-glacial stratigraphy by thin subaerial deposits (e.g., fluvial sediments and soil) overlying the glacial and glaciomarine deposits (Domack, 1984; Demet et al., 2019).

**Text S2.** Detailed text outlining OSL sample collection, processing, and age determination.

### S2.1 Sample collection and preparation

Sediment samples were collected across unit boundaries with coarse-grain quartz material. In order to avoid pre-mature bleaching OSL, samples were collected before sunrise or after sunset, were only exposed to low energy red light, and were wrapped in opaque black plastic before being transported to East Carolina University (ECU) for preparation and processing. Sample preparation was carried out under dark-room conditions using standard coarse-grain procedures: samples were wet-sieved at 90-125 µm with some expansion to grain sizes of 63-212 µm. After drying the samples at 50 °C, the samples were treated with 10 % hydrochloric acid (HCl) and 29 % hydrogen peroxide ($H_2O_2$). A high-density separation was conducted with lithium heteropolytungstate (LST) at a density of 2.72-2.75 g/cm$^3$ to isolate quartz grains. Coarse grains were etched for 40 minutes with 48% hydrofluoric acid (HF) to remove outer parts affected by alpha radiation, followed by a 10% HCl rinse to remove fluoride precipitates. A low-density separation to isolate quartz from feldspar was conducted with LST at a density of 2.62 g/cm$^3$. After final sieving, the aliquots were prepared by using Reusch Silkospray to adhere material to the stainless steel sample cups.

Bulk sediment was collected from outcrops for gamma spectrometry measurements and stored for at least 4 weeks prior to measurement. While the OSL samples were taken at unit boundaries, the dose rate samples were taken from the same unit as the OSL samples. Therefore, the gamma dose rates reflect the sample unit only and contain no information about adjacent, underlying, or overlying units.

### S2.2 Age determination

Dose measurements were conducted using a Risø TL/OSL-DA-20 reader manufactured by Risø National Laboratory with a bialkali PM tube (Thorn EMI 9635QB). The built-in $^{90}$Sr/$^{90}$Y beta source gives a dose rate of ~100 mGy/s. Optical stimulation was carried out with an IR LED array at 870 nm with 121 mW/cm$^2$ (90 %) power at the sample, a blue LED array at 470 nm with 74 mW/cm$^2$ (90 %) power at the sample and a 7.5 mm Hoya U-340 detection filter (290-370 nm; Bøtter-Jensen & Murray, 1999). Equivalent doses were determined following the single-aliquot regenerative dose (SAR) procedure developed by Murray and Wintle (2000) and Wintle and Murray (2006). Due to feldspar contamination, a post-IR procedure was used to isolate quartz signals in the equivalent dose measurements (Wallinga et al., 2002). The preheat temperature of 180 °C for 10 s was determined for each sample using plateau and dose recovery tests. Our specific measurement protocol is outlined in Table 2. Luminescence signals $L_i$ and $T_i$ were determined by integrating over the first 0.8 seconds of an OSL decay curve and subtracting an average of the next 4 seconds as background signal. The signal uncertainty followed from counting statistics. The sensitivity corrected signal is given by $C_i = L_i/T_i$. The dose response of every aliquot was determined by fitting the luminescence signals $C_1$ to $C_5$ with a saturating exponential. The dose $D_0$ corresponding to the natural sensitivity-corrected luminescence signal $C_0$, was calculated with the fitting parameters. All uncertainties were calculated using the Gaussian law of error propagation and Poisson statistics. The vast majority of aliquots passed the reliability test – requiring recycling ratios between 0.9 and 1.1, dose recovery <10 % deviation from given dose, low recuperation. The equivalent dose $D_e$ was determined for each site using the central age model (Galbraith, 1999). The full uncertainty also includes 3.1 % for the built-in beta source error.

In the sediment, grains are exposed to natural gamma and beta radiation from uranium, $^{232}$Th, and potassium. The concentrations of these radionuclides were measured with high resolution gamma spectrometry. Uranium concentrations determined from $^{234}$Th were all significantly higher than concentrations determined from $^{214}$Pb and $^{214}$Bi. We assumed that $^{234}$U was leached out of the sample due to in situ water presence.

Dose rates were calculated by using the actual measured concentrations for the nuclides in the uranium decay chain. Uncertainties were calculated based on the maximum and minimum values obtained from the measured concentrations of $^{234}$Th and $^{214}$Bi/$^{214}$Pb. Water contents were very low and have an uncertainty of 5 % (Table 2). Beta and gamma dose rates were calculated using the conversion factors published by Guérin et al. (2011). The cosmic dose rate was calculated as described by Prescott and Stephan (1982), Barbouti and Rastin (1983), and Prescott and Hutton (1994) and incorporates site latitude, longitude, site altitude, and sample depth below surface. The effective thickness was assumed to be half the burial depth with uncertainty of 5 %.

The sample ages, calculated in calendar years, were calculated by dividing the dose by the dose-rate (Table 2). Due to feldspar contamination in some samples, fading was measured with a post-IR blue sequence for all samples. Only some of the samples showed fading. For those, the ages were corrected as suggested by Auclair et al. (2003). While $^{14}$C ages are reported in kilo years ago (kya) calendar year BP (1955), all OSL ages are reported in kya based on the date of collection (2020). OSL ages in kya can be directly compared to kya cal. BP by subtracting 72 years from the OSL age.


**Figure S1.** A clay lamination seen in Unit 3 of Fort Casey Site 1 (left) and a silt lens seen in Unit 1 of Fort Casey Site 1 (right). This distinction is maintained throughout all site stratigraphic descriptions.

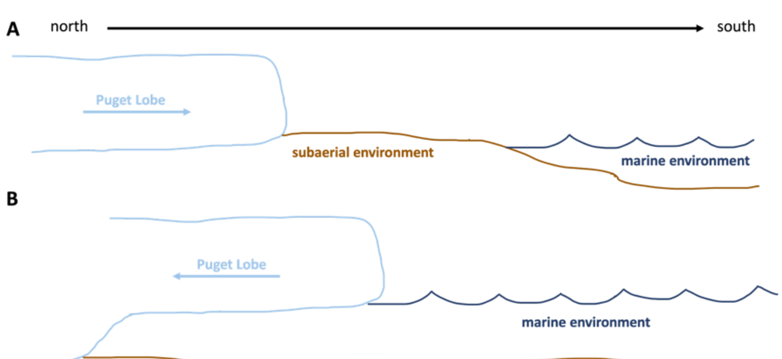


**Figure S2.** Schematic drawing of A) time 1 indicating Puget Lobe advance into subaerial Puget Lowland post landscape emergence (Figure 2). B) Indicates time 2 Puget Lobe ice retreat within a marine environment post landscape-submergence and marine-incursion following time 1. Puget Lobe ice retreat in a marine environment only occurred at southernmost sites Double Bluff and Penn Cove (Figure 2).

**Table S1.** Site and sample collection information.

| Site | Sediment samples | Radiocarbon samples | OSL samples |
|---|---|---|---|
| Double Bluff (a) | 53 | 2 | 0 |
| Fort Casey (b) | 20 | 0 | 2 |
| Penn Cove (c) | 126 | 8 | 2 |
| West Beach (d) | 54 | 4 | 6 |
| Cliffside (e) | 29 | 0 | 0 |
| **Total** | **282** | **14** | **12** |

**Table S2.** OSL measurement sequence

1. Radiation dose $D_i$
2. Preheat at 180°C* for 10s
3. IRSL at 125°C for 150s to remove feldspar signal
4. OSL at 125°C for 100s, measure OSL signal $L_i$
5. Fixed test radiation dose $D_t$**
6. Cutheat at 160°C to remove unstable signals
7. IRSL at 125°C for 150s to remove feldspar signal
8. OSL at 125°C for 100s, measure OSL signal $T_i$
9. Repeat steps 2-8 for cycle 0 and steps 1-8 for cycles 1-7

Cycle 0: Natural signal, $D_0 = 0$ Gy with no administered dose
Cycle 1-5: Regenerative doses, $D_1$, $D_2<D_1<D_3<D_0<D_4<D_5$
Cycle 6: Dose recovery test, $D_6=D_4$***
Cycle 7: Recycle test, $D_7=D_1$***
Cycle 8: Recuperation test, $D_8=0$

* preheat temperature determined by plateau test
** $D_t$= 15-20% $D_0$
*** administered to check the precision with which a known dose can be recovered